

T-2432

HIGH TEMPERATURE HEAT TRANSPORT
IN POROUS MEDIA
APPARATUS DESIGN AND TESTING

by

Salim Skaff

ARTHUR LAKES LIBRARY
COLORADO SCHOOL of MINES
GOLDEN COLORADO 80401

CLOSED RESERVE

ProQuest Number: 10782237

All rights reserved

INFORMATION TO ALL USERS

The quality of this reproduction is dependent upon the quality of the copy submitted.

In the unlikely event that the author did not send a complete manuscript and there are missing pages, these will be noted. Also, if material had to be removed, a note will indicate the deletion.



ProQuest 10782237

Published by ProQuest LLC (2018). Copyright of the Dissertation is held by the Author.

All rights reserved.

This work is protected against unauthorized copying under Title 17, United States Code
Microform Edition © ProQuest LLC.

ProQuest LLC.
789 East Eisenhower Parkway
P.O. Box 1346
Ann Arbor, MI 48106 – 1346

T-2432

A thesis submitted to the faculty and Board of Trustees of the Colorado School of Mines in partial fulfillment of the requirements for the degree of Master of Science in Chemical and Petroleum-Refining Engineering.

Signed: 

Golden, Colorado

Date: April 27, 1981

Approved by:


Dr. Michael C. Jones
Advisor


Dr. Phillip F. Dickson
Head of Department

Golden, Colorado

Date: April 27, 1981

ABSTRACT

This thesis describes the design, construction and testing of an apparatus for the measurement of the interphase heat transfer coefficient in packed beds at high temperatures and low Reynolds numbers.

The interphase heat transfer coefficient has to be inferred from the transient response of the bed to a perturbation in the temperature of the gas entering the bed. The model used is the one suggested by Vortmeyer and Shaefer (1) with a term added to account for the heat loss from the bed. The model contains a Peclet number (Pe), which is the summation of the convective and conductive heat transport occurring in the bed.

The temperature profiles generated by the numerical solution of the model, for different values of Pe are compared to the experimental profiles and the sum of the square of the differences are computed. The value of Pe that results in the least deviation is chosen.

Results show that the model used can predict the experimental temperature profiles, furthermore, the value of Pe determined from the model compares favorably to the values calculated using correlations available in the literature for the effective axial thermal conductivity of the bed with no flow (λ_e^0) and the Nusselt number, terms contained in the

expression of Pe . The Pe is determinable only if the heat lost from the bed is minimized.

It can therefore be concluded that the apparatus built and the data reduction scheme are capable of determining an interphase heat transfer coefficient provided that the value of λ_e^0 is known accurately from an independent measurement.

TABLE OF CONTENTS

	<u>Page</u>
ABSTRACT.	iii
LIST OF FIGURES	vii
LIST OF TABLES.	viii
ACKNOWLEDGEMENTS.	ix
INTRODUCTION.	1
THEORY.	2
APPARATUS	11
I. Design Considerations.	11
II. Apparatus Construction	12
PRELIMINARY EXPERIMENTAL CHECKS	18
I. Channeling	18
II. Rotameter Calibration.	19
III. Thermocouple Calibration	19
EXPERIMENTAL PROCEDURE.	22
DATA REDUCTION PROCEDURE.	23
RESULTS	29
DISCUSSION OF RESULTS	45
ERROR ANALYSIS.	46
CONCLUSIONS	49
RECOMMENDATIONS	50
NOMENCLATURE.	51
REFERENCES.	54

TABLE OF CONTENTS (cont.)

	<u>Page</u>
APPENDIX.	
A. Derivation of the One Phase Model.	57
B. Solid Properties	62
C. Fluid Properties	67
D. Insulation Properties.	69
E. Computer Program	72

LIST OF FIGURES

<u>Figure</u>	<u>Page</u>
1. Schematic Diagram of Apparatus.	13
2. Diagram of Bed.	16
3. Rotameter Calibration Curve	20
4. Thermocouple Calibration Curves	21
5. Sample Error Map for Run #4	24
6. Sample Error Map for Run #1	25
7. General Shapes of Error Maps.	26
8. Results for Run #1.	41
9. Results for Run #2.	42
10. Results for Run #3.	43
11. Results for Run #4.	44
12. Solid Thermal Expansion Curves.	65
13. Thermal Conductivity of Insulation.	71

LIST OF TABLES

<u>Table</u>	<u>Page</u>
1. Experimental Results for Run #1.	30
2. Experimental Results for Run #2.	31
3. Experimental Results for Run #3.	33
4. Experimental Results for Run #4.	35
5. Fitted Polynomical Coefficients.	37
6. Experimental Conditions.	38-39
7. Derived Results.	39
8. Calculated Pe.	39
9. Percent Difference Between Calculated and Measured Pe.	40
10. λ_e^0/λ_g for Different Correlations	41

ACKNOWLEDGEMENTS

I would like to express my sincere appreciation to Dr. Michael C. Jones for his valuable guidance and suggestions throughout all phases of this study. Also Drs. Philip F. Dickson, E. Dendy Sloan and Michael S. Graboski for their participation on the thesis defense committee.

T-2432

TO MY PARENTS

x

INTRODUCTION

The knowledge of interphase heat transfer coefficients in packed beds at low Reynolds numbers is essential in many areas of chemical engineering, specifically in oil shale retorts, coal and biomass gasifiers and regenerative heat exchangers in coal fired MHD converters. All the above processes involve temperatures higher than or equal to 760K (900 °F) where radiative heat transfer is important if not dominating.

The overall objective of this project is to investigate the radiative interphase heat transfer process in packed beds as it applies to oil-shale retorting. It is shown in reference (9) that in conditions similar to those encountered in oil-shale retorts, radiative heat transfer may be the predominant mode of heat transfer.

The scope of this investigation is to design, build and test an apparatus for the measurement of interphase heat transfer coefficients and to develop a suitable data reduction scheme. This work is limited to purely convective solid-fluid heat transfer. Future work will include radiative as well as convective heat transfer based on the conclusions and recommendations of this investigation.

Results obtained by other investigators (2,6,14) show the interphase heat transfer coefficient and therefore the

the Nusselt number as a function of the Reynolds number (2), both the Reynolds number and the Prandtl number (6) or the Reynolds number, the Prandtl number and the void fraction of the bed (14).

Interphase heat transfer coefficient data for packed beds, at low Reynolds numbers, until 1979 are reviewed in references (6,18,19). It is to be noted that the available experimental data are all at low temperatures where radiation is unimportant, moreover there is considerable disagreement in the reported results. Different investigators developed different correlations for the Nusselt number as a function of the Reynolds number. These correlations do not yield comparable results, in fact the differences between the values they predict tend to increase as the Reynolds number decreases; hence the difficulty of comparing experimental results at low Reynolds number. It appears that the differences are due to the different models used in interpreting experimental data.

THEORY

Direct measurement of interphase heat transfer coefficients requires measurement of heat fluxes and interphase temperature differences. The interphase heat transfer coefficient is then:

$$h = q/\Delta T$$

where h is the heat transfer coefficient, q is the heat flux and ΔT the driving force. In the case where strong radiation is occurring, either solid to solid or solid to fluid, the temperature of the fluid is not measurable, therefore heat transfer coefficients cannot be measured directly; they have to be inferred by other means.

Interphase heat transfer coefficients in packed beds can be calculated indirectly from the dynamic response of the bed to an induced perturbation of the temperature of the fluid. The perturbation can be a pulse, a step, or an oscillation. The calculation is made possible by use of a mathematical model that describes the packed bed and enables the prediction of the experimental results. Therefore, the results are somewhat dependent on the model used as pointed out by (1,6,14).

Many models have been used by different investigations in the study of heat transfer in packed beds. Most models are basically two-phase models, i.e. there are two heat

balances, one for each phase; the solid phase and the fluid phase. Each model is based on some assumptions which may or may not be applicable in all cases. Some of these models are:

1) The Schumann model (6)

$$\frac{\partial T_F}{\partial t} = -v' \frac{\partial T_F}{\partial x} - \frac{ha}{\epsilon C_F \rho_F} (T_F - T_S) \quad *$$

$$(1 - \epsilon) \frac{\partial T_S}{\partial t} = \frac{ha}{C_S \rho_S} (T_F - T_S)$$

The Schumann model assumes that the fluid is in plug flow, no temperature gradient exists within the particle, and it neglects axial conduction in the solid phase.

2) The Continuous Solid model (C-S) (6):

$$\frac{\partial T_F}{\partial t} = \frac{K_{ef}}{\epsilon C_F \rho_F} \frac{\partial^2 T_F}{\partial x^2} - v' \frac{\partial T_F}{\partial x} - \frac{ha}{C_F \rho_F} (T_F - T_S)$$

$$(1 - \epsilon) \frac{\partial T_S}{\partial t} = \frac{k_{es}}{C_S \rho_S} \frac{\partial^2 T_S}{\partial x^2} + \frac{ha}{C_S \rho_S} (T_F - T_S)$$

The Continuous Solid model assumes that the fluid is in dispersed plug flow, and that there is also axial heat conduction in the solid phase which is continuous. It is again assumed that no temperature gradients exist within the solid.

*All symbols are defined in nomenclature p. (51).

T-2432

3) The Dispersion Concentric model (D-C) (6):

$$\frac{\partial T_F}{\partial t} = \alpha_{ax} \frac{\partial^2 T_F}{\partial x^2} - \frac{\partial T_F}{\partial x} - \frac{ha}{\epsilon C_F \rho_F} (T_F - T_S(R))$$

$$\frac{\partial T_S}{\partial t} = \alpha_s \left(\frac{\partial^2 T_S}{\partial r^2} + \frac{2}{r} \frac{\partial T_S}{\partial r} \right)$$

with the boundary condition:

$$\text{@ } r = R \quad K_s \frac{\partial T_S}{\partial r} = h (T_F - T_S)$$

The Dispersion concentric model assumes that the fluid is in dispersed plug flow and the solid particle temperature field has radial symmetry. Particle to particle heat transfer is ignored.

Each of the previous three models is an attempt to realistically represent a packed bed.

The Schumann model does not take into account dispersion which becomes important at low flow rates. The C-S model on the other hand includes the dispersion effects and internal heat conduction in the solid phase. The D-C model (6) calculates an average particle temperature from the concentric profile and uses it as a local solid temperature.

For present purposes at high temperatures, where significant particle to particle heat transfer may be present

due to radiation, the C-S model seems most appropriate. Experiments can be designed so that the disregard of particle internal temperature gradients is unimportant, namely by the use of small diameter particles. Littman and Sliva (2) have shown that a packed bed can be represented by the C-S model with the dispersion term in the gas phase neglected. The two phase heat balance equations are now the following:

$$\epsilon \rho_F C_F \frac{\partial T_F}{\partial t} = - G C_F \frac{\partial T}{\partial x} + h a (T_S - T_F)$$

$$(1-\epsilon) \rho_S C_S \frac{\partial T_S}{\partial t} = (1-\epsilon) K_{es} \frac{\partial^2 T_S}{\partial x^2} + h a (T_F - T_S)$$

Vortmeyer and Shaefer (1) have reduced the Littman and Sliva model from two phases to one phase based on the assumptions that the thermal capacity of the fluid is much smaller than that of the solid and also that the second partial derivatives of the fluid and solid phases with respect to x are equal. A sufficient condition for the later assumption is that the fluid and solid temperatures be almost equal.

The one phase model becomes:

$$(1-\epsilon) \rho_S C_S \frac{\partial T_S}{\partial t} = (\lambda_e^0 + \frac{G^2 C_F^2}{h a}) \frac{\partial^2 T}{\partial x^2} - G C_F \frac{\partial T}{\partial x} \quad (1)$$

A derivation of the one-phase model is shown in Appendix A.

If a heat loss term is included to account for heat lost from the bed equation 1 becomes

$$(1-\epsilon) \rho_S C_S \frac{\partial T_S}{\partial t} = \left(\lambda_e^0 + \frac{G^2 C_F^2}{ha} \right) \frac{\partial T_S}{\partial x^2} - GC_F \frac{\partial T_S}{\partial x} - h' b (T_S - T_0)$$

where T_0 is the average temperature of the surroundings.

In the perturbed dimensionless form the above equation becomes:

$$\frac{\partial \theta}{\partial t^*} = \frac{1}{Pe(1-\epsilon)} \frac{\partial^2 \theta}{\partial x^{*2}} - \gamma \frac{\partial \theta}{\partial x} - H\theta \quad (2)$$

The derivation of the above equation is shown in Appendix A.

The boundary conditions for the one phase model with step input in gas temperature at the inlet of the bed are:

$$\theta \text{ at } x^* = 0 \text{ (inlet of the bed)}$$

$$GC_F (1 - \theta) = - \frac{\lambda a x}{D_p} \frac{\partial \theta}{\partial x^*}$$

and $\theta \text{ at } x^* = L/D_p \text{ (outlet of the bed)}$

$$\frac{\partial \theta}{\partial x} = 0$$

The boundary conditions are known as the Danckwerts boundary conditions. At the inlet, a heat balance is made

T-2432

on a differential bed length. At the outlet, the boundary condition implies that there is no temperature gradient at the end of the bed. The reasoning behind that is that if there were a gradient it would be either positive or negative. If it were positive then for heating, the temperature profile would pass through a minimum somewhere in the bed, and if it were negative a heat balance shows that the gas temperature outside the bed would be higher than the gas temperature at the exit of the bed. Neither case can occur; therefore, the gradient must be zero at the outlet of the bed. Bischoff (22) has shown how these boundary conditions may be arrived at by detailed analysis. It is to be noted that the accumulation term in the outlet boundary condition may be neglected because the differential volume can be made infinitesimally small and because the thermal capacity of the fluid is small relative to that of the bed.

The assumptions made in the derivation of the Vortmeyer model are justifiable in the present experiments: the fluid physical properties such as heat capacity, density, and thermal conductivity are all much smaller than those of the solid. Calculations show that the particle temperature becomes equal to the gas temperature in a time much smaller than the time it takes the temperature front to cross one particle diameter. The penetration time for the temperature to reach the center of the spheres is about 0.5 second; whereas the time required

for the temperature front to traverse one particle diameter ranges from 50 to 100 seconds. Therefore, assuming the solid temperature equal to the fluid temperature is a good assumption. The calculations mentioned above are for a particle diameters of about 1.8 mm and a mass flow rate range from 1.5×10^{-4} to 3.0×10^{-4} kg/s.

Solution of the one phase model (equation 2) yields temperature profiles as a function of time and the axial direction for given assumed values of Pe and H. In equation (2), Pe represents the ratio of the convective to "diffusive" heat transfer, γ is the volumetric heat capacity ratio and H is equivalent to a number of transfer units for heat loss.

The Pe contains the terms: λ_e^0 , the effective thermal conductivity of the solid phase with stagnant gas. Correlations for the values of λ_e^0 are given in the literature (3,4, 5). h is the interphase heat transfer coefficient, it could be due to convection only or a contribution of both convection and radiation. A possible assumption in the case where both convective and radiative interphase heat transfer are present is that:

$$h = h_{\text{conv}} + h_{\text{rad}}$$

h_{rad} is proportional to T^3 , but for a small temperature perturbation it can be assumed constant. \hat{a} , is the area of solid per unit volume and for spheres is equal to:

$$a = 6 (1-\epsilon)/D_p$$

An advantage of Vortmeyer's one phase model over other models is its simplicity and its ease of solution. This is not done at the expense of accuracy of the solution as compared to other models. It is shown in reference (1) that the one phase model yields results that are comparable to results obtained by other models.

APPARATUS

I. Design Considerations

Since radiative heat transfer becomes important at high temperatures and since the calculation of the interphase heat transfer coefficient requires the transient response of a packed bed to a perturbation in the gas temperature, the apparatus should be able to withstand the operating temperature and enable the perturbation to be induced. Also the design should consider the assumptions made in the mathematical model and try to meet the conditions necessary to make these assumptions valid.

High temperature materials have to be used in order to satisfy the operating temperature requirements. Spherical particles are to be used because of the ease of calculation of the surface area per unit volume. The particle diameter has to be small relative to the bed diameter in order to minimize solid to solid radiation and reduce the possibility of channeling. This also decreases the time constant of the particle, so that the penetration depth of perturbation is equal to or greater than the average particle radius in a time smaller than that taken by the temperature front to move one particle diameter. As mentioned, earlier the latter condition is satisfied.

The reduction of the particle diameter reduces solid to solid radiation because the geometric mean beam length, ℓ_m , is decreased. Reference (9) shows that the radiative contribution to the thermal conductivity of the bed is directly proportional to ℓ_m . Also, small spheres reduce the possibility of channeling because they create many more paths for gas flow and reduce voidage variations at walls and intrusions like thermocouples.

The wall thickness of the vessel holding the packing should be small so as to make the heat content of the walls small relative to the heat capacity of the bed.

II. Apparatus Construction

A schematic diagram of the apparatus is shown in Figure 1. The gas supply (in this case a non-radiating gas; nitrogen) passes through a rotameter on its way to the heater. The gas flow is designed to enable a stream of cold gas to bypass the furnace. The stream could later on be cut off by means of a toggle valve to allow a step increase in the gas temperature to enter the bed. The total flow through the bed remains unchanged because the supply valve, {2} is chosen so that the gas velocity at the orifice is sonic, this makes the flow rate independent of the downstream pressure.

T-2432

The heater, {11}, a "Harper Electric Furnace" with a hollow carbon heating element rated at 8 kw and a maximum temperature of 1900 K (3000 °F), is used to heat the gas before it enters the bed {10}. This is achieved by means of three meters of (0.25" x 0.035") Inconel tubing placed inside the heater in the form of hairpin sections, five passes in all.

The packing in the bed consists of "Coors Ceramic" AD-90 spherical granules (their mean diameter is 1.837 mm) whose composition and properties are listed in Appendix B. A 2.5" layer of 1/4" spheres is placed at the inlet of the bed to evenly distribute the gas flow. The temperature in the bed is measured by three thermocouples. The junctions of two {T1, T2} are placed on the centerline of the bed 103 mm apart, the third junction {T3} is placed at the wall adjacent to T2. T3 is used to measure the temperature difference between the center and the wall of the bed. The bed and all the hot tubing are insulated with a high temperature insulation, Johns Manville "Cerachrome" that can withstand temperatures of about 1700 k (2600 °F). The thermal conductivity of this material is given in Appendix D. The bed and all the hot tubing, except the heat exchanger, are made of 304 stainless steel. All tubing connections are made with 1/4", 316 stainless steel "Swagelok" fittings.

The furnace temperature is controlled by a "Honeywell" SCR {9} acting on the secondary transformer relay switch of the furnace. The SCR is driven by a "Honeywell" proportional controller {8} calibrated to give 0-100% output for an inlet voltage range of 41.269 mV to 48.828 mV, which corresponds to a temperature range of 1273 to 1473 K (1830 to 2190 °F). The furnace temperature is measured with a thermocouple (T4). Temperature control to within ± 0.25 K. The gas temperature exiting the furnace is measured with a thermocouple (T5). All thermocouples are standard type-K (Chromel-Alumel).

The bed consists of an 8" x 2" O.D., 304 stainless steel tube with 0.012" wall. A schematic diagram of the bed is shown in Figure 2. The bed and insulation are placed in a 55 gal steel drum. A cylindrical guard heater {12} of 9.5" in diameter and 18" in length surrounds the bed. The power input to the guard heater can be varied by means of a Variac. The insulation temperature at the guard is monitored by a thermocouple (T6). The guard heater is used to minimize heat loss from the bed and therefore minimize the steady state temperature gradient in the bed.

A heating coil {14} is wound, in the insulation, around the tubing as it exits the furnace to minimize the heat loss from the gas before it reaches the bed.

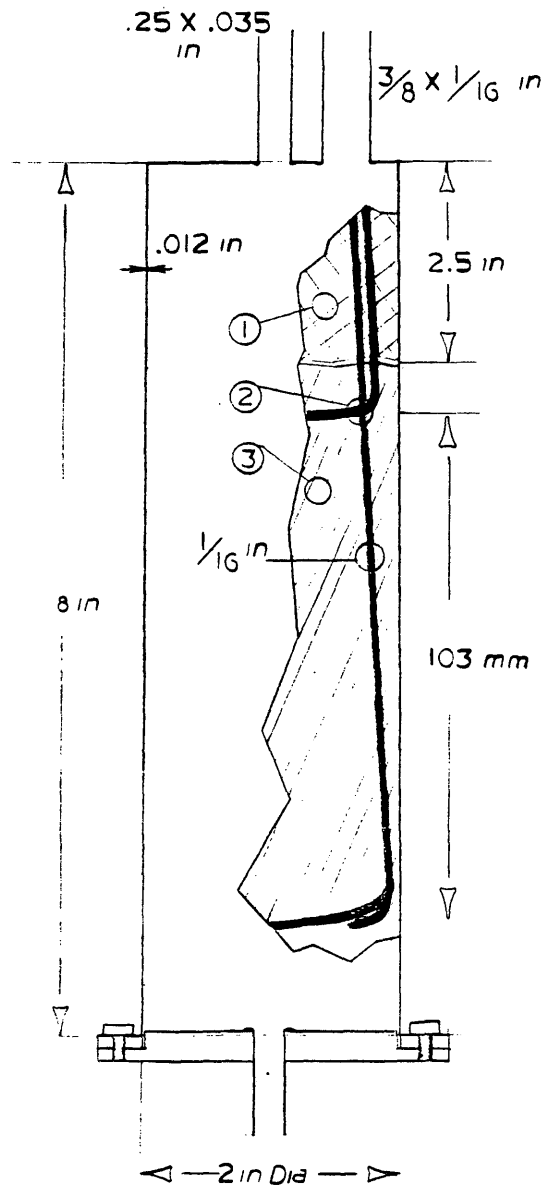


Figure 2. DIAGRAM OF THE BED

1. 1/4" spheres
2. Thermocouples
3. 1.837 mm spheres

T-2432

All thermocouples are connected to a panel and selector switch, which in turn is connected to a "Keithley Digital Multimeter" via an "Omega CJ" cold junction compensator. The multimeter precision is $1 \mu\text{V}$ and it is accurate to $\pm 4 \mu\text{V}$, in the range of measurements (25 to 30 mV).

PRELIMINARY EXPERIMENTAL CHECKSI. Channeling

Pressure drops across the bed were calculated for the experimental flow rate range and were found to be small (10) (less than 5 mm Hg). The pressure drop was measured at a much higher flow rate in two cases; first, when thermocouples T1, T2 and T3 were placed in the bed, second, when no thermocouples were present. Measurements showed that the pressure drop in both cases was identical (within the readability of the manometer). The precision of the reading was 1.3 mm of mercury, corresponding to an accuracy of about 1.8% in the range of the value of the pressure drop. This was evidence that the presence of the thermocouples did not cause significant changes in the flow characteristics of the bed. Further evidence could be obtained by observation of the bed thermocouples. If wall channeling were occurring T3 should have shown an increase in temperature before T2. On the other hand, if there were channeling in the center of the bed the converse should have been observed. Moreover if there were channeling along the thermocouple wire, then T2 and T3 should have started changing as soon as T1. None of the above conditions was encountered during the experimental runs.

II. Rotameter Calibration

The main flow rotameter was calibrated using a "Precision Scientific Company" wet test meter. The reading in the rotameter is at 30 psig, pressure at which all of the experimental runs were performed. The flow is at 620 mm of mercury and 70⁰F. Figure 3 shows the calibration curve. The manufacturer's calibration curve showed that the flow rate was directly proportional to the reading (at 1 atm and 70⁰F).

III. Thermocouple Calibration

The thermocouples used in the experiment were calibrated against a reference chosen at random from the group. The procedure was to bundle the thermocouples and place them in the furnace at different temperatures. At room temperature, all thermocouples read the same to within $\pm 1 \mu\text{V}$ of each other.

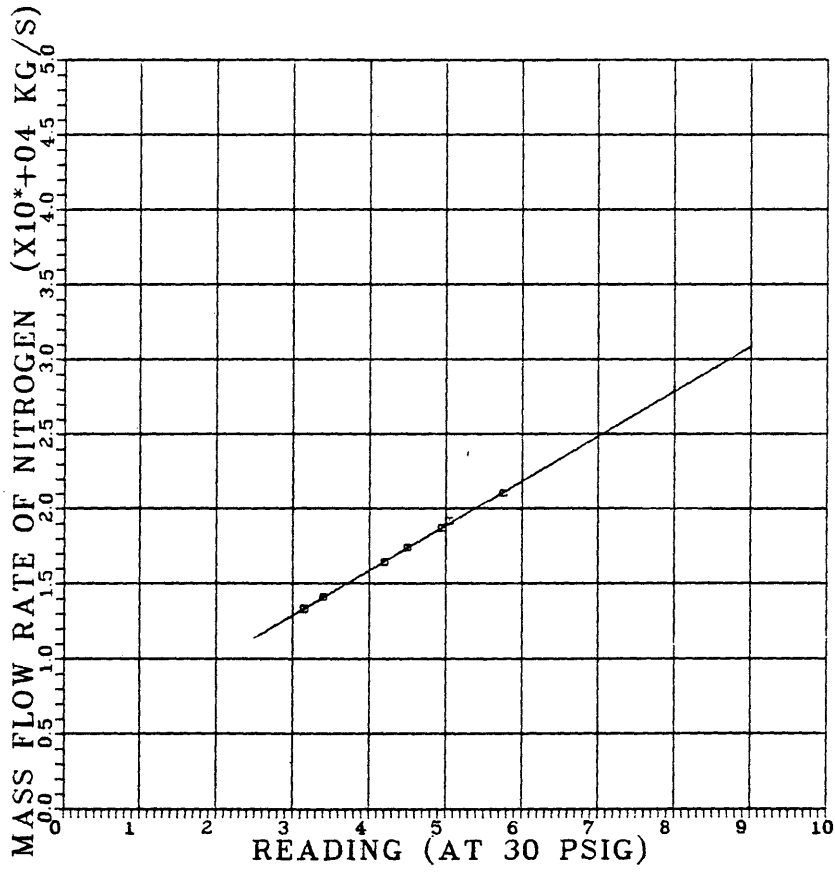


Figure 3. ROTAMETER CALIBRATION CURVE

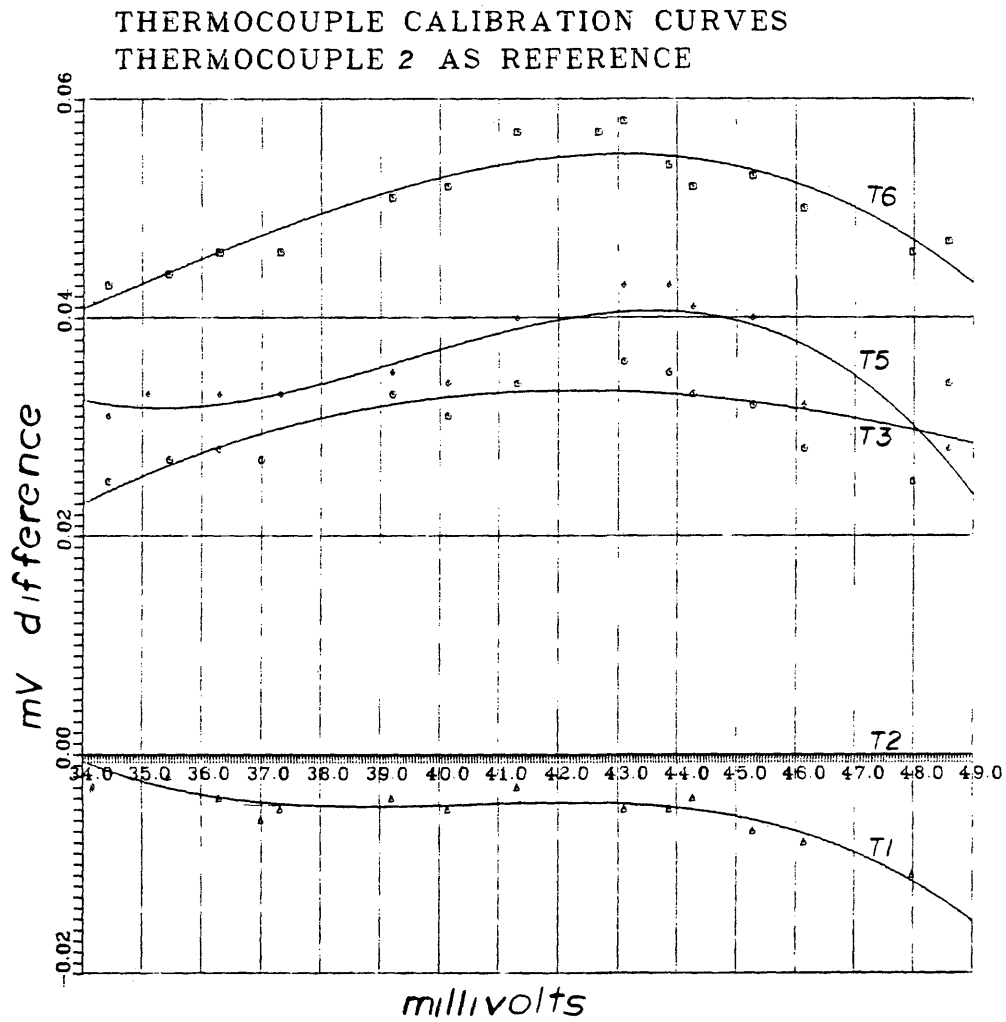


Figure 4. CALIBRATION CURVES FOR THERMOCOUPLES

EXPERIMENTAL PROCEDURE

After the furnace has reached steady state, the gas supply is turned on and the bed is heated to steady state with the bypass valve open. Both the guard heater and the heating coil are switched on at the beginning of the experiment.

When steady state is reached, as shown by the thermocouples placed in the bed, the chart recorder is switched on and the bypass valve is shut.

The change in temperature at the inlet of the bed is recorded as well as the difference between the inlet and outlet thermocouples. The values of the inlet temperature are read periodically directly from the digital multimeter because the values plotted on the chart recorder are not accurate enough due to the high ranges setting required on the recorder for the inlet temperatures. The temperature difference is read off the chart and is accurate to 0.05% in the experimental range.

The experiment is continued until the rate of change of the temperature with time is small compared to the maximum change.

DATA REDUCTION PROCEDURE

The experimental data were first reduced to a dimensionless form. A numerical solution to the one phase model was developed using the implicit method. A copy of the computer program used and details pertaining to its solution are in Appendix E. Initial solutions of the one phase model with a step increase at the inlet of the bed compared poorly to the experimental responses of T2. The most important reason was the presence of the layer of large spheres which caused dispersion in the heat wave, thereby changing its shape.

A more successful approach was as follows. The reduced experimental profiles were fitted to a polynomial. The polynomial for T1 was used as the forcing function for the numerical solution. The generated output profile at T2 was then compared to the experimental output and the Euclidian norm was computed for different pairs of values of Pe and H. The Euclidian norm is defined as the sum of the squares of the differences between the generated and experimental responses of T2.

$$e = \sum_{i=1}^n (T_{\text{calc}} - T_{\text{exp}})^2$$

An "error" map was drawn for each run in order to locate the values of Pe and H that best fit the data.

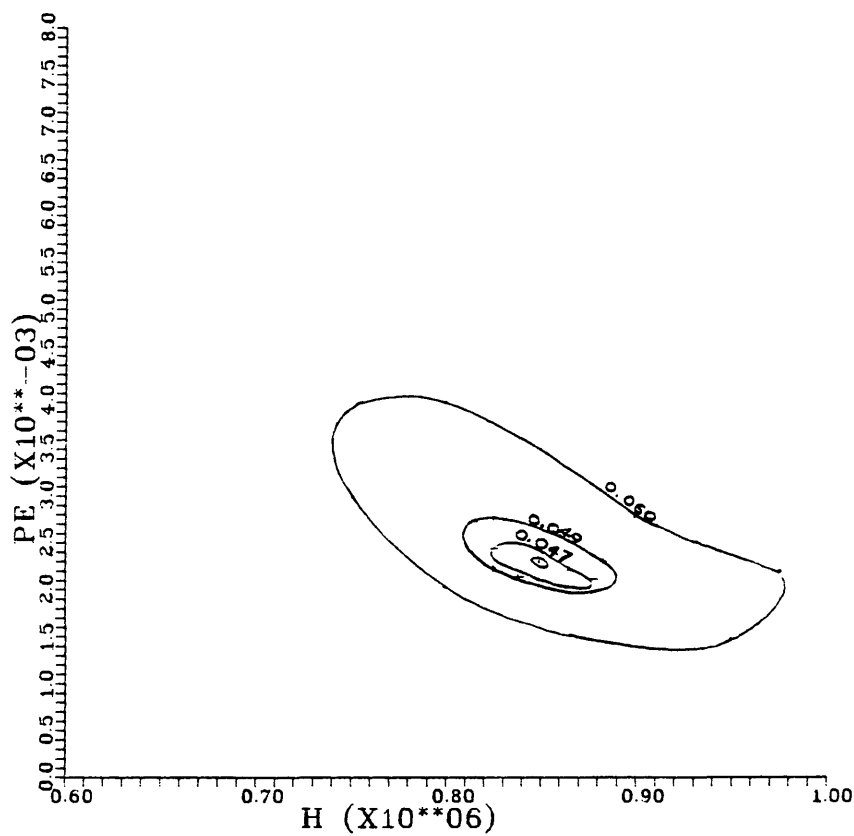


FIGURE 5. SAMPLE ERROR MAP FOR RUN 4

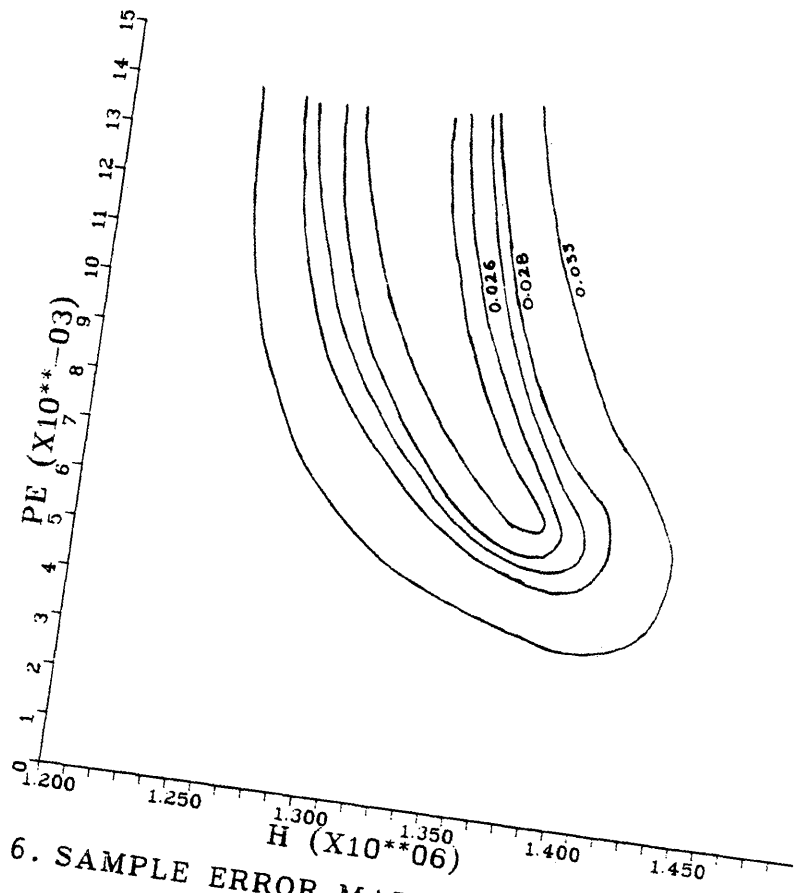


FIGURE 6. SAMPLE ERROR MAP FOR RUN 1.

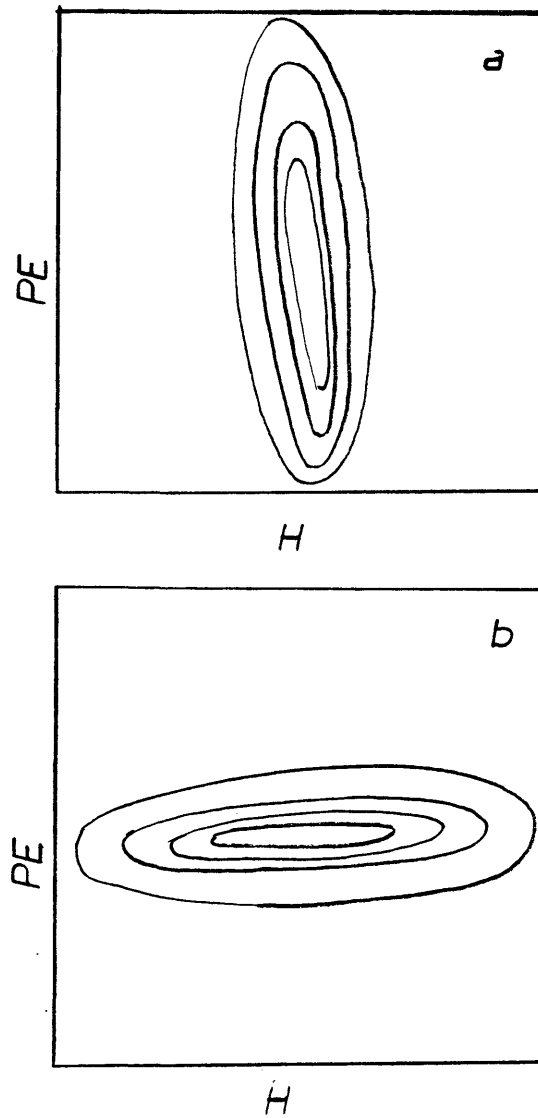


Figure 7. GENERAL SHAPES
OF ERROR MAPS
- Dependence of error on:
a- H
b- Pe

For comparison, theoretical values for Pe were calculated using the following equation derived in Appendix A.

$$1/Pe = \frac{\lambda_e^0}{\lambda_g} \frac{\gamma(1-\epsilon)}{Re Pr} + \frac{Re Pr \gamma}{6 Nu}$$

Values of λ_e^0/λ_g were estimated using different correlations from references (3,4,5), as were values of Nu (2,6). The values of λ_e^0/λ_g were calculated with solid to solid and void to void radiative heat transfer taken into account. The equations used are listed below:

From reference (3)

$$\lambda_e^0/\lambda_g = (\lambda_s/\lambda_g)^{0.280 - 0.757 \log \epsilon - 0.057 \log (\lambda_s/\lambda_g)} \quad (3)$$

The above equation does not account for the radiative contribution. From reference (5) the radiative contribution (λ_r^0/λ_g) was calculated and added to the value obtained from the equation of reference (3)

$$\lambda_r^0 = 0.692 \rho D_p T^3/10^8 \quad (3A)$$

Where T is in degrees Fahrenheit and λ_r^0 in (Btu/ft - hr - °F).

From reference (5):

$$\lambda_e^0/\lambda_g = \beta(1-\epsilon)/(\sigma (\lambda_g/\lambda_s) + 1/(1/\phi + D_p h_{rs}/\lambda_g) + \epsilon \beta D_p h_{rv} / \lambda_g) \quad (4)$$

where h_{rs} , the solid-solid radiative heat transfer coefficient, is equal to:

$$h_{rs} = 0.1952 (p/(2 - p)) \cdot (T/100)^3$$

and h_{rv} , the void-void radiative heat transfer coefficient, is equal to:

$$h_{rv} = 0.1952 / \left(\left(1 + \frac{\epsilon}{2(1-\epsilon)} \right) \cdot \frac{1-p}{p} \right) \cdot (T/100)^3$$

where T is in Kelvin, h_{rv} and h_{rs} are in $\text{Kcal/m}^2 \cdot \text{hr.K}$

$$\phi = 0.04, \quad \beta = \sigma = 1.0$$

The correlations for the Nusselt number used were:

From reference (2)

$$\text{Nu} = 0.89 \text{Re}^{0.41} \quad 0.6 < \text{Re} < 13 \quad (5)$$

and from reference (6)

$$\text{Nu} = 2 + 1.1 \text{Re}'^{0.6} \text{Pr}^{1/3} \quad (6)$$

Re is based on the superficial velocity of the gas whereas Re' is based on the interstitial velocity.

RESULTS

Figures 8,9,10 and 11 show the experimental, fitted and where possible, generated temperature responses for T1 and T2 for the values of Pe and H listed in Table 8. Tables 1, 2, 3 and 4 are tabulations of the experimental results. Table 5 shows the fitted polynomial coefficients for T1 and T2. Values of Pe and H were obtained from runs #3 and #4. The first two runs yielded no results as discussed below. Tables 6 and 7 represent the experimental conditions for each run. Values of the calculated Pe, for different correlations mentioned earlier, are listed in Table 9. Column I uses values of λ_e^0/λ_g calculated from equation 3 with the radiation contribution calculated from the difference in equation 4 when h_{rs} and h_{rv} are evaluated and when they are ignored. Column II uses values of λ_e^0/λ_g calculated from equation 3 with 3A. Column III uses values of λ_e^0/λ_g calculated from equation 4. Sub-columns (5) use values of Nu calculated from equation 5. Sub-columns (6) use values of Nu calculated from equation 6. Table 10 represents the percent difference between the measured and calculated Pe for different correlations of λ_e^0/λ_g and Nu.

Table 1. Results for Run #1

<u>t*(x10⁻⁴)</u>	<u>θ inlet</u>	<u>θ outlet</u>
0.00	0.000	0.000
7.14	-0.004	0.000
9.24	-0.025	0.000
12.18	-0.051	0.000
15.54	-0.089	0.000
18.91	-0.145	0.000
21.01	-0.190	0.000
33.19	-0.402	0.000
47.05	-0.597	-0.053
63.44	-0.740	-0.155
76.46	-0.813	-0.250
86.54	-0.856	-0.318
98.31	-0.898	-0.390
114.69	-0.941	-0.471
121.83	-0.961	-0.499
142.00	-0.975	-0.551
145.78	-0.978	-0.561
183.17	-0.998	-0.621
198.89	-1.000	-0.627

Table 2. Results of Run #2

<u>t*</u>	<u>θ inlet</u>	<u>θ outlet</u>
0.00	0.000	0.000
3.28	0.001	0.000
6.93	0.016	0.000
10.95	0.056	0.000
14.60	0.113	0.000
17.52	0.166	0.000
21.53	0.245	0.000
25.18	0.317	0.000
28.83	0.384	0.007
33.94	0.469	0.014
37.59	0.522	0.027
41.60	0.574	0.048
48.54	0.651	0.092
53.28	0.695	0.127
57.66	0.730	0.160
61.31	0.755	0.188
67.51	0.792	0.236
68.61	0.798	0.244
71.16	0.812	0.263
74.81	0.829	0.290
78.64	0.845	0.316
81.74	0.858	0.337

Table 2. (cont.)

<u>t*</u>	<u>θ inlet</u>	<u>θ outlet</u>
85.76	0.872	0.358
89.41	0.885	0.384
93.06	0.896	0.404
96.71	0.906	0.423
100.40	0.915	0.442
104.00	0.924	0.458
107.70	0.931	0.473
111.70	0.939	0.490
115.00	0.945	0.501
118.60	0.952	0.514
122.30	0.958	0.527
125.90	0.963	0.538
129.60	0.968	0.552
133.20	0.973	0.561
137.20	0.978	0.571
140.50	0.982	0.579
143.10	0.987	0.588
148.20	0.991	0.597
151.80	0.994	0.603
155.10	0.998	0.609
156.90	1.000	0.614

Table 3. Results of Run #3

<u>t*</u>	<u>θ inlet</u>	<u>θ outlet</u>
0.00	0.000	0.000
1.67	0.002	0.001
3.33	0.005	0.002
5.00	0.010	0.003
6.66	0.016	0.004
8.33	0.025	0.004
9.99	0.037	0.006
11.66	0.051	0.007
13.32	0.070	0.008
14.99	0.089	0.009
16.65	0.112	0.009
19.98	0.165	0.011
21.65	0.192	0.012
32.47	0.379	0.020
34.14	0.406	0.022
38.30	0.470	0.031
46.63	0.580	0.058
50.79	0.627	0.078
54.12	0.660	0.099
59.95	0.711	0.139
70.77	0.786	0.227
73.27	0.800	0.250

Table 3. Cont.

<u>t*</u>	<u>θ inlet</u>	<u>θ outlet</u>
78.27	0.826	0.294
82.43	0.845	0.329
87.42	0.866	0.373
91.59	0.881	0.407
96.58	0.897	0.445
101.60	0.911	0.480
106.60	0.924	0.511
111.60	0.936	0.541
119.10	0.950	0.581
126.60	0.963	0.617
129.10	0.967	0.627
130.70	0.970	0.634
133.20	0.973	0.643
142.40	0.985	0.678
144.00	0.987	0.684
146.50	0.990	0.692
155.70	0.999	0.716
156.50	1.000	0.719

Table 4. Results of Run #4

<u>t*</u>	<u>θ inlet</u>	<u>θ outlet</u>
0.00	0.000	0.000
2.63	0.006	0.000
5.26	0.012	0.000
7.89	0.022	0.000
10.52	0.036	0.012
15.78	0.080	0.018
18.41	0.112	0.023
21.04	0.146	0.029
24.20	0.192	0.034
27.36	0.237	0.039
31.57	0.300	0.047
34.20	0.338	0.053
39.46	0.409	0.067
44.72	0.475	0.087
47.88	0.510	0.097
52.61	0.559	0.125
57.87	0.606	0.155
63.13	0.647	0.189
68.40	0.682	0.224
73.66	0.713	0.261
78.92	0.740	0.297
84.18	0.763	0.331

T-2432

Table 4. Cont.

<u>t*</u>	<u>θ inlet</u>	<u>θ outlet</u>
89.44	0.784	0.366
97.33	0.812	0.410
105.20	0.836	0.456
113.10	0.857	0.496
121.00	0.875	0.526
128.90	0.891	0.558
135.70	0.903	0.583
145.20	0.920	0.609
152.60	0.931	0.631
161.00	0.943	0.657
171.50	0.957	0.676
179.40	0.970	0.694
187.30	0.980	0.710
197.30	0.991	0.728
207.30	1.000	0.744

Table 5. Thermocouple Polynomial Coefficient

<u>RUN</u>	<u>1</u>	<u>2</u>	<u>3</u>	<u>4</u>
A ₀	0.39344 x 10 ⁻²	-0.14646 x 10 ⁻²	0.68027 x 10 ⁻²	0.14210 x 10 ⁻¹
A ₁	0.44842 x 10 ⁻²	-0.41035 x 10 ⁻²	-0.52279 x 10 ⁻²	-0.23715 x 10 ⁻²
A ₂	-0.98979 x 10 ⁻³	0.12038 x 10 ⁻²	0.10242 x 10 ⁻²	0.63287 x 10 ⁻³
A ₃	0.20242 x 10 ⁻⁴	-0.28829 x 10 ⁻⁴	-0.21574 x 10 ⁻⁴	-0.11222 x 10 ⁻⁴
A ₄	-0.18065 x 10 ⁻⁶	0.30158 x 10 ⁻⁶	0.20346 x 10 ⁻⁶	0.86356 x 10 ⁻⁷
A ₅	0.76030 x 10 ⁻⁹	-0.14947 x 10 ⁻⁸	-0.92295 x 10 ⁻⁹	-0.31354 x 10 ⁻⁹
A ₆	-0.12287 x 10 ⁻¹¹	0.28572 x 10 ⁻¹¹	0.16345 x 10 ⁻¹¹	0.43864 x 10 ⁻¹²

Outlet Thermocouple Polynomial Coefficients

B ₀	-0.32127	0.29836	-0.33689 x 10 ⁻²	0.30515 x 10 ⁻²
B ₁	0.24939 x 10 ⁻¹	-0.26498 x 10 ⁻¹	0.28022 x 10 ⁻²	0.15025 x 10 ⁻²
B ₂	-0.62014 x 10 ⁻³	0.75387 x 10 ⁻³	-0.22513 x 10 ⁻³	-0.76417 x 10 ⁻⁴
B ₃	0.54711 x 10 ⁻⁵	-0.77192 x 10 ⁻⁵	0.66615 x 10 ⁻⁵	0.31741 x 10 ⁻⁵
B ₄	-0.21697 x 10 ⁻⁷	0.36107 x 10 ⁻⁷	-0.64278 x 10 ⁻⁷	-0.33478 x 10 ⁻⁷
B ₅	0.32682 x 10 ⁻¹⁰	-0.64856 x 10 ⁻¹⁰	0.25685 x 10 ⁻⁹	0.14307 x 10 ⁻⁹
B ₆	-	-	-0.35995 x 10 ⁻¹²	-0.22064 x 10 ⁻¹²

$$\theta = \sum_{i=0}^6 S_i t^i$$

S_i = A_i for inlet
 = B_i for outlet
 θ is dimensionless temperature
 t* is dimensionless time x 10⁻⁴
 i = 0, 1, 2, ..., 6

θ is dimensionless temperature

TABLE 6. EXPERIMENTAL CONDITIONS (KELVINS)

Run	Initial Temperature			Final Temperature			Guard Heater	
	T	T2	T3	T1	T2	T3	T6	T6
1	926.2	863.7	857.0	846.2	813.7	809.0	766	756
2	815.5	784.7	779.3	917.7	845.4	839.0	746	762
3	914.4	878.7	873.4	1054.7	977.9	974.0	771	796
4	877.7	883.6	882.0	932.3	924.4	922.0	856	877

TABLE 7. EXPERIMENTAL CONDITIONS

Run	Mass Flow Rate (Kg/s)	T1 (K)	T2 (K)
1	1.7×10^{-4}	926.15	863.65
2	1.5×10^{-4}	815.50	784.70
3	3.0×10^{-4}	914.40	878.65
4	2.0×10^{-4}	877.70	883.60

TABLE 8. DERIVED RESULTS

Run	Re	Pe	H
1	3.88	-	-
2	3.46	-	-
3	6.25	4563	$.7875 \times 10^{-6}$
4	4.38	2281	$.8500 \times 10^{-6}$

TABLE 9. CALCULATED Pe FOR DIFFERENT CORRELATIONS OF λ_e^0/λ_g AND Nu

Run	I		II		III	
	(5)	(6)	(5)	(6)	(5)	(6)
3	3749	4335	3897	4693	3169	3677
4	2654	2890	2844	3116	2304	2479

TABLE 10. PERCENT DIFFERENCE BETWEEN
CALCULATED AND MEASURED Pe FOR DIFFERENT
CORRELATIONS OF λ_e^0/λ_g AND Nu

Run	I		II		III	
	(5)	(6)	(5)	(6)	(5)	(6)
3	-21.7	-5.3	-17.1	2.8	-44.0	+24.1
4	14.1	21.1	19.8	26.8	0.10	8.0

TABLE 11. λ_e^0/λ_g FOR
DIFFERENT CORRELATIONS

Run	I	II	III
1	12.660	11.786	14.609
2	12.708	11.795	14.615
3	12.181	11.199	14.481
4	12.442	11.510	14.567

RESULTS FOR RUN 1, EXPERIMENTAL
AND FITTED.

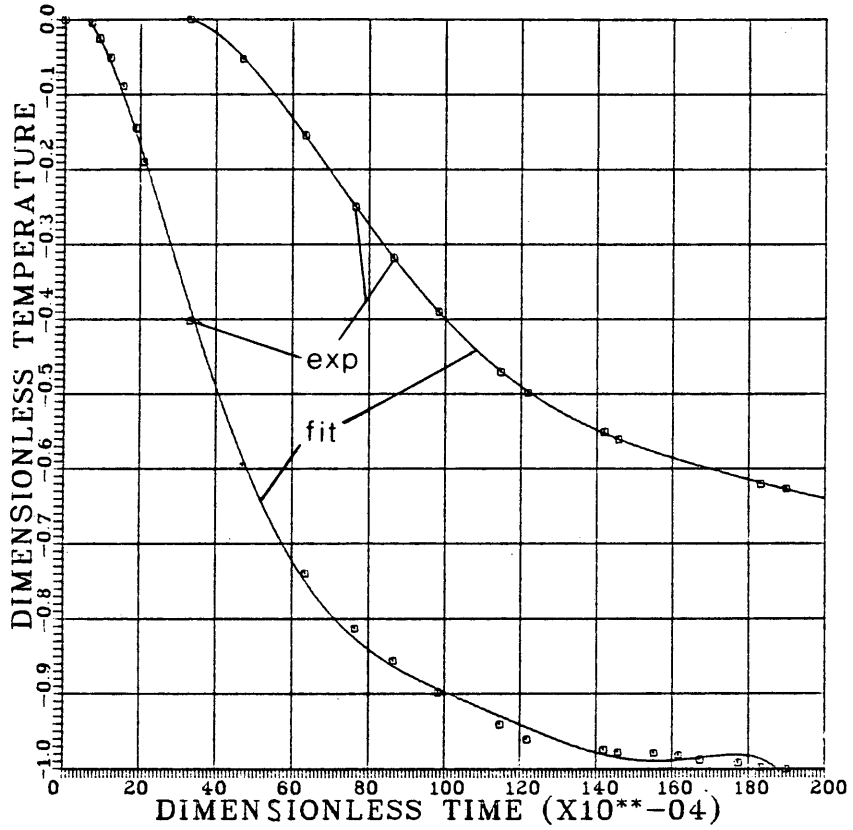


FIGURE 8. RESULTS FOR RUN 1

RESULTS FOR RUN 2, EXPERIMENTAL
AND FITTED.

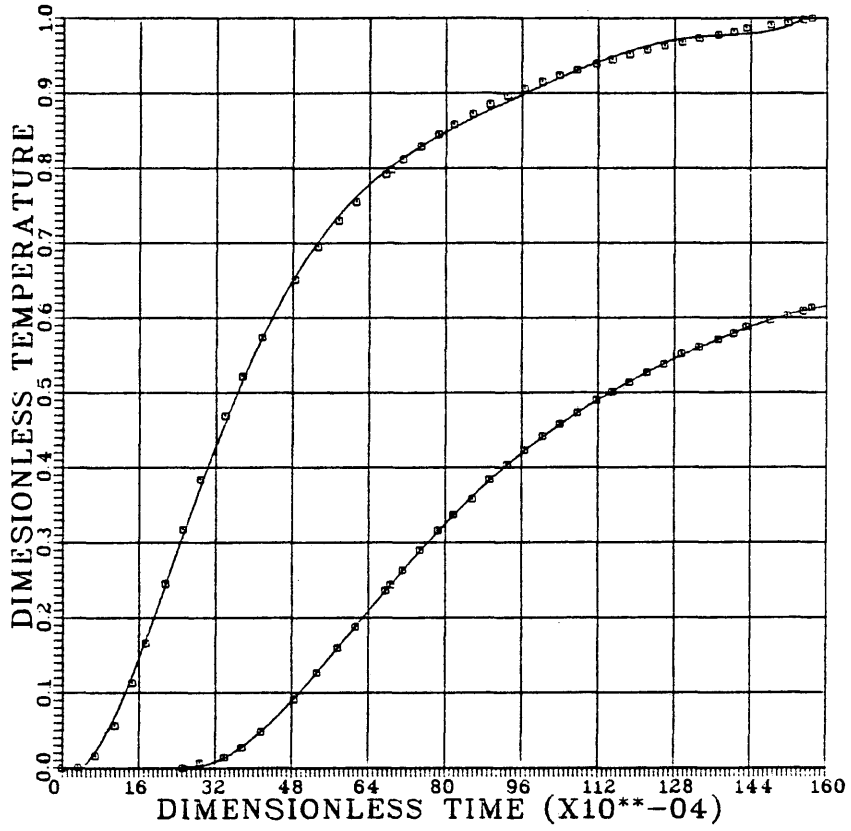


FIGURE 9. RESULTS FOR RUN 2

RESULTS FOR RUN 3, EXPERIMENTAL
FITTED AND CALCULATED. PE=4563.

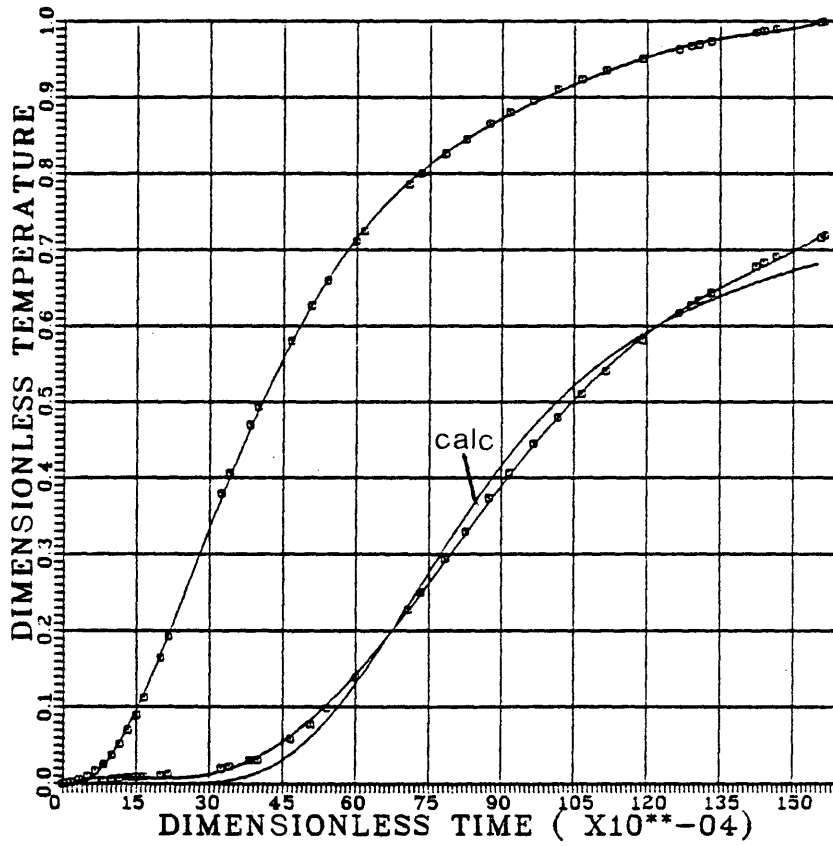


Figure 10. RESULTS FOR RUN 3

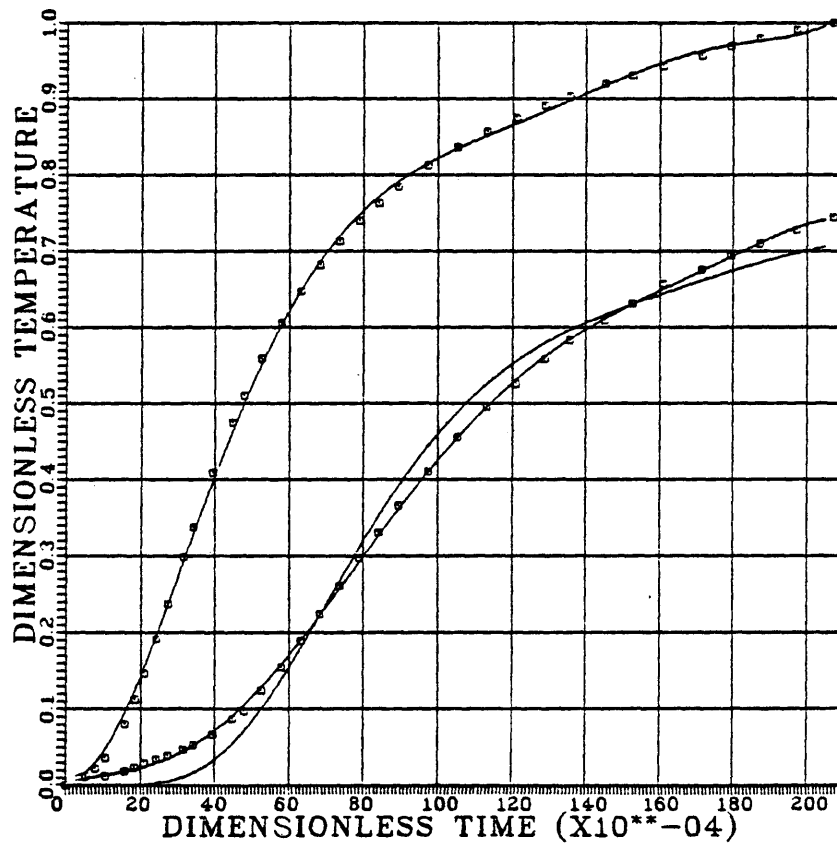
RESULTS FOR RUN 4, EXPERIMENTAL
FITTED AND CALCULATED. PE=2281.

FIGURE 11. RESULTS FOR RUN 4

DISCUSSION OF RESULTS

The values obtained for Pe in runs #3 and #4 seem to compare favorably with the values calculated using the different correlations for λ_e^0/λ and Nu .

Sample error maps with constant Euclidian norm contours for runs #1 and #4 are shown in Figures 5 and 6. The maps for runs #1 and #2 showed that the error was a stronger function of H than Pe , while the maps for runs #3 and #4 showed the converse. The shapes of the error contours in the cases mentioned above were significantly different. Figure 7 shows the general shapes of the error map in the cases when: H is predominant, such as for run #1 and #2, and when the dependence of the error is dominated by Pe , such as for runs #3 and #4.

In trying to examine the possible reasons that caused Pe to be undetermined for the first two runs, a conclusion was reached based on the following observations:

- 1) The first three runs were conducted with the same power input into the guard heater.
- 2) The last run was conducted with double the power input into the guard heater.
- 3) The heat loss term H , is inversely proportional to the velocity.
- 4) Run #3 had the highest flow rate.

5) The flow rate in runs #1, #2 and #4 did not vary significantly. Observations 2 and 5 imply that the only significant difference between the first two runs and the last was the power input into the guard heater. Observations 1 and 4 imply that the main difference between the first three runs was the flow rate. Observation 3 implies that the difference between the first three runs was the heat loss coefficient, H . The only common factor between runs #3 and #4 was that in both cases the heat loss coefficient, H , was reduced. For run #3, H decreased because the power input to the guard heater increased hence decreasing the heat loss from the bed.

This leads to the tentative conclusion that $(H\theta)$ has to be small compared to $(1/Pe (1-\epsilon) \partial^2\theta/\partial x^2)$ in equation 2 for Pe to be determined.

It is to be noted that while relative errors of the fit calculated from the Euclidean norms are quite small, (1.7% for run #3 and 2.4% for run #4) inspection of the fits reveals that the model produces a shape which is consistently wrong. This could be a limitation of the model. Further testing with different models may reveal which of the neglected parameters is responsible.

ERROR ANALYSIS

I. Error in the dimensionless temperature

- o The numerical solution

The time and space intervals were reduced until the generated temperature profiles were constant to the third significant digit. This was equivalent to a relative error of 0.001 or 0.1%.

- o The experimental data

The values of the dimensionless temperatures were calculated from the ratio of the temperature change at time t to the total change in temperature at the inlet of the bed. The relative error was equal to about 0.1%.

- o The fitted experimental data

The experimental data were fitted into a polynomial form. The error introduced was less than 0.1%

- o The generated solution

The average relative error calculated from the Euclidian norm was 1.7% for run #3 and 2.4% for run #4. The average error was calculated by taking the square root of the ratio of the Euclidian norm to the number of temperature differences used to calculate it. Therefore it may be seen that the deviation between the generated solution and experimental data was large relative to the other errors in temperature.

II. Error in Pe

The Peclet number that yielded the minimum error was determined in a range of $\pm 0.4\%$ for run #3 and 0.7% for run #4.

III. Error in dimensionless time ($=tD_p/v$)

The dimensionless time was calculated using the actual time, and the superficial gas velocity, and the average particle diameter. The gas velocity was calculated from the mass flow rate which was read off the rotameter. The error in the velocity equaled the error in the mass flow rate. The relative error in the mass flow rate was determined by the readability of the rotameter ($1/2$ division/100), which corresponded to an error of 0.5% , and the accuracy of the wet test meter. A reasonable figure of the latter would be about 0.5% . The mean particle diameter was calculated from the solid density and the average mass of a sphere. The relative error in the mass of the sphere is about 0.5% and the overall error in dimensionless time is about 1.5% . It is to be noted that the error in the dimensionless time will not affect the deviation between the generated and experimental responses.

CONCLUSIONS

From the results obtained, it may be concluded that the apparatus built and the data reduction scheme used are capable of determining a Peclet number in reasonable agreement with the values calculated using the various correlations of λ_e^0/λ_g and Nusselt number.

Calculations have shown that the value of the Nusselt number inferred from the Pe data was strongly dependent on the value of λ_e^0/λ_g assumed, and that the range of values of λ_e^0/λ_g obtained from different correlations yielded a very wide range of Nusselt numbers (-33.7 to 5.9 for run #3 and 0.67 to 1.7 for run #4). Therefore the value of λ_e^0/λ_g has to be known more accurately, preferably from an independent measurement.

The one phase model seemed to be able to predict the experimental temperature profiles when Pe was determined. The determinability of Pe depended on the magnitude of the dimensionless heat loss transfer coefficient H. When H was larger than about 1.0×10^{-6} (in the experimental conditions ranges), Pe was undetermined.

RECOMMENDATIONS

From the results and conclusions of the experiments it is recommended to:

1. Increase the diameter of the bed in order to minimize the relative heat loss from the bed. A larger diameter bed has a smaller wall area to volume ratio.
2. Add more thermocouples to the bed in order to have more details about the temperature profiles in the bed.
3. Conduct runs for:
 - a. Same temperature and different flow rates.
 - b. Same flow rate and different temperatures.

This will enable the comparison of different runs with only one parameter change at a time.

4. Increase the residence time of the gas in the heat exchanger and allow for a higher gas temperature to be reached.
5. Decrease the distance between the furnace and the bed to minimize heat loss from the gas before it reaches the bed.

NOMENCLATURE

a	Solid area per unit volume of bed (m^{-1})
b	Gas-wall contact area per unit length of bed (m)
c	Heat capacity (J/kg.k)
D_p	Mean particle diameter (m)
G	Gas mass velocity (K_g/m^2 .)
h	Interphase heat transfer coefficient (W/m^2-K)
h'	Heat loss coefficient (W/m^2-K)
H	Dimensionless heat loss coefficient
h_{conv}	Convective interphase heat transfer coefficient
h_{rad}	Radiative interphase heat transfer coefficient
h_{rs}	Solid-solid radiative heat transfer coefficient
h_{rv}	Void-void radiative heat transfer coefficient
K_e	Effective thermal conductivity
L	Length of bed
Nu	Nusselt number (hD_p/λ_f)
ρ	Emissivity of solid
Pe	Peclet number (Lv/α_{eax})
Pr	Prandtl number
Re	Reynolds number based on superficial velocity ($\rho v D_p/\mu$)
Re'	Reynolds number based on interstitial velocity ($\rho v' D_p/\mu$)
T	Temperature
$T_{-\infty}$	Gas inlet temperature

t	Time
v_s	Superficial velocity
v'	Interstitial velocity
x	Axial distance variable

Greek Symbols

α_{eax}	Effective axial thermal diffusivity of bed
α_{eF}	Axial fluid thermal dispersion coefficient
α	Thermal diffusivity
β	Ratio of effective length between centers to particle diameter
σ	Ratio of effective length of solid relating to thermal conduction to the particle diameter
ϕ	Ratio of the effective thickness of fluid film adjacent to contact surface of two solid particle to the particle diameter
ϵ	Bed void fraction
ρ	Density
λ	Thermal conductivity
γ	Volumetric heat capacity ratio of fluid and solid
μ	Viscosity of fluid

Subscripts

s	Solid
F	Fluid
e	Effective
ax	Axial
g	Gas

Superscripts

o	No flow
*	Dimensionless

T-2432

REFERENCES

1. Vortmeyer, D. and Schaefer, R., Chem. Eng. Sci, 1974 29, pp. 485-491.
2. Littman, H. and Sliva, E., 4th Int. Heat Transfer Conference, Paris-Versailles 1970, Vol. 7.
3. Krumpiczka, R., Int. Chem. Eng., 1967 7 p. 122.
4. Yagi, S. and Kunii, D., A.I.Ch.E. J., 1957 3 (3), pp. 373-381.
5. Schotte, W., A.I.Ch.E. J., 1960 6 (1), pp. 63-67.
6. Wakao, N., et al., Chem. Eng. Sci., 1979 34, pp. 325-336.
7. NBS Technical Note 648, Thermophysical Properties of Nitrogen, 1973.
8. NBS Monograph 125, Thermocouple Reference Tables, Based on the I PTS-68, 1974.
9. Jones, M. C., Research Proposal, January 1980.
10. Bird, R., Stewart, W., and Lightfoot, E., Transport Phenomena, John Wiley and Sons, Inc., New York, 1960, p. 198.
11. Carnahan, B., et al., Applied Numerical Methods, John Wiley and Sons, Inc., New York, 1969, pp. 441.
12. Touloukian, Y., Buyco, E., "Thermophysical Properties of Matter, Vol. 5, IFI/Plenum Press, New York, 1970, pp. 25, 57, 140, 210.
13. Coors Poreclain Company, Bulletin No. 953.
14. Gunn, D. J., Int. J. Heat and Mass Transfer, 1978. 21, pp. 467-476.
15. Vortmeyer, D., Chem. Eng. Sci., 1975, 30, pp. 999-1001.
16. Seese, T. and Thomson, W., Ind. Eng. Chem., Process Des. Dev., 1977, 16, (2) pp. 243-248.
17. Hottel, H., Sarafim, A., Radiative Transfer, McGraw-Hill Company, New York, 1967, p. 148.

18. Balakrishnan, R. and Pei, T., *Ind. Eng. Chem. Process Dev.*, 1979, 18 (1), pp. 30-50.
19. Handley, D. and Heggs, P., *Trans. Instn, Chem. Engrs.*, 1968, 46, pp. T251-T264.
20. Danckwerts, P. V., *Chem, Eng. Sci.*, 1953, 2 (1), pp. 1-13.
21. Villadsen, J. and Michelsen, M., Solution of Differential Equation Models by Polynomial Approximation, Prentice-Hall International Series, pp. 15-20, (1978).
22. Bischoff, K. B., *Chem. Eng. Sci.*, 1961, 16, p. 731.

APPENDIX A
DERIVATION OF THE ONE PHASE MODEL

APPENDIX A

I. Derivation of the one-phase model with heat loss.

1. 2-phase energy equations

$$\text{Gas } \epsilon \rho_F C_F \frac{\partial T_g}{\partial t} = - GC_F \frac{\partial T_g}{\partial x} + ha(T_s - T_g) + h'b(T_o - T_g)$$

$$\text{Solid } (1-\epsilon) \rho_S C_S \frac{\partial T_s}{\partial t} = ha(T_g - T_s) + (1-\epsilon)K_{es} \frac{\partial^2 T_s}{\partial x^2}$$

$(1-\epsilon)K_{es}$ is of the same order of magnitude as λ_e^0 (1).

Assume thermal capacity of fluid is small compared to thermal capacity of solid,

$$0 = + GC_F \frac{\partial T_g}{\partial x} + ha(T_g - T_s) - h'b(T_o - T_g) \quad (1A)$$

$$(1-\epsilon)\rho_S C_S \frac{\partial T_s}{\partial t} = ha(T_g - T_s) + \lambda_e^0 \frac{\partial^2 T_s}{\partial x^2} \quad (2A)$$

Subtracting 1A from 2A

$$\begin{aligned} (1-\epsilon)\rho_S C_S \frac{\partial T_s}{\partial t} &= \lambda_e^0 \frac{\partial^2 T_s}{\partial x^2} - GC_F \frac{\partial T_g}{\partial x} + h'b(T_o - T_g) \\ &+ GC_F \frac{\partial T_s}{\partial x} - GC_F \frac{\partial T_s}{\partial x} \\ &= \lambda_e^0 \frac{\partial^2 T_s}{\partial x^2} - GC_F \frac{\partial (T_g - T_s)}{\partial x} - GC_F \frac{\partial T_s}{\partial x} \quad (3A) \end{aligned}$$

T-2432

From equation 1A

$$-\frac{\partial(T_g - T_s)}{\partial x} = \frac{GC_F}{ha} \frac{\partial^2 T_g}{\partial x^2} - \frac{h'b}{ha} \partial \frac{(T_o - T_g)}{\partial x}$$

Substituting in 3A

$$(1-\epsilon)\rho_s C_s \frac{\partial T_s}{\partial t} = \lambda_e^o \frac{\partial^2 T_s}{\partial x^2} + GC_F \left(\frac{GC_F}{ha} \frac{\partial^2 T_g}{\partial x^2} \right. \\ \left. - \frac{h'b}{ha} \frac{\partial(T_o - T_g)}{\partial x} \right) - GC_F \frac{\partial T_s}{\partial x} + h'b(T_o - T_g)$$

Assume:

$$T_s = T_g$$

$$\frac{\partial^2 T_s}{\partial x^2} = \frac{\partial^2 T_g}{\partial x^2}$$

$$(1-\epsilon)\rho_s C_s \frac{\partial T_s}{\partial t} = \left(\lambda_e^o + \frac{G^2 C_F^2}{ha} \right) \frac{\partial^2 T_s}{\partial x^2} + \frac{h'b}{ha} GC_F \frac{\partial T_s}{\partial x}$$

$$- GC_F \frac{\partial T_s}{\partial x} + h'b(T_o - T_s)$$

$$= \left(\lambda_e^o + \frac{G^2 C_F^2}{ha} \right) \frac{\partial^2 T_s}{\partial x^2} + \left(\frac{h'b}{ha} - 1 \right) GC_F \frac{\partial T_s}{\partial x}$$

$$+ h'b(T_o - T_s)$$

$$\frac{h'b}{ha} \ll 1;$$

Therefore:

$$(1-\epsilon)\rho_s C_s \frac{\partial T_s}{\partial t} = \left(\lambda_e^0 + \frac{G^2 C_F^2}{ha}\right) \frac{\partial^2 T_s}{\partial x^2} - GC_F \frac{\partial T_s}{\partial x} - h'b (T_s - T_0) \quad (4A)$$

II. Perturbation Analysis

Assume $T_s = T_{ss} + T'$

where T_{ss} is the steady state temperature and T' is the perturbation.

Let:

$$\lambda_e^0 + \frac{G^2 C_F^2}{ha} = \lambda_{ax}$$

Equation 4A becomes

$$(1-\epsilon)\rho_s C_s \frac{\partial (T_{ss} + T')}{\partial t} = \lambda_{ax} \frac{\partial^2 (T_{ss} + T')}{\partial x^2} - GC_F \frac{\partial (T_{ss} + T')}{\partial x} - h'b(T_{ss} + T' - T_0) \quad (5A)$$

at steady state equation 5A becomes

$$0 = \lambda_{ax} \frac{\partial^2 T_{ss}}{\partial x^2} - GC_F \frac{\partial T_{ss}}{\partial x} - h'b (T_{ss} - T_0) \quad (6A)$$

Subtracting 6A from 5A we get:

$$(1-\epsilon)\rho_s C_s \frac{\partial T'}{\partial t} = \lambda_{ax} \frac{\partial^2 T'}{\partial x^2} - GC_F \frac{\partial T'}{\partial x} - h' b T' \quad (7A)$$

III. Dimensionless form

Define:

$$t^* = \frac{tv}{D_p}; \quad x^* = \frac{x}{D_p}, \quad \theta = \frac{T' - T'_{-\infty}}{T'_{-\infty}}$$

where $T'_{-\infty}$ is the maximum amplitude of the perturbation,

Equation 7A becomes:

$$(1-\epsilon)\rho_s C_s \frac{v}{D_p} \frac{\partial \theta}{\partial t^*} = \frac{\lambda_{ax}}{D_p^2} \frac{\partial^2 \theta}{\partial x^{*2}} - \frac{GC_F}{D_p} \frac{\partial \theta}{\partial x^*} - h' b \theta \quad (8A)$$

Dividing 8A by $(1-\epsilon)\rho_s C_s v/D_p$ we get

$$\frac{\partial \theta}{\partial t^*} = \frac{\lambda_{ax}}{\rho_s C_s D_p v (1-\epsilon)} \frac{\partial^2 \theta}{\partial x^{*2}} - \frac{GC_F}{(1-\epsilon)\rho_s C_s v} \frac{\partial \theta}{\partial x^*} - \frac{h' b D_p}{(1-\epsilon)\rho_s C_s v} \theta \quad (9A)$$

Define

$\lambda_{ax}/\rho_s C_s = \alpha_{eax}$; the effective axial thermal diffusivity of the solid

T-2432

$Pe = D_p v / \alpha_{eax}$; the Peclet number based on the particle diameter.

$$\gamma = \frac{\rho_F C_F}{\rho_S C_S (1-\epsilon)} ; \text{ the volumetric heat capacity ratio}$$

$H = \frac{h' b D_p}{\rho_S C_S (1-\epsilon) v}$; the dimensionless heat loss coefficient.

Equation 9A becomes

$$\frac{\partial \theta}{\partial t^*} = \frac{1}{Pe(1-\epsilon)} \frac{\partial^2 \theta}{\partial x^{*2}} - \gamma \frac{\partial \theta}{\partial x^*} - H \theta \quad (10A)$$

IV. Pe as a function of dimensionless groups

Pe is defined as:

$$Pe = D_p v / \alpha_{eax}$$

$$\alpha_{eax} = (\lambda_e^0 + G^2 C_F^2 / ha) / \rho_S C_S$$

Therefore: $Pe = D_p v \rho_S C_S / (\lambda_e^0 + G^2 C_F^2 / ha)$

or

$$\frac{1}{Pe} = \frac{\lambda_e^0}{D_p v \rho_S C_S} + \frac{G^2 C_F^2}{ha D_p v \rho_S C_S} \quad (11A)$$

multiplying and dividing by $\rho_F \mu C_F \lambda_g$ and substituting a for $6(1-\epsilon)/D_p$ equation 11A becomes

$$\frac{1}{Pe} = \frac{\lambda_e^0}{\lambda_g} \frac{\gamma(1-\epsilon)}{Re Pr} + \frac{Re Pr \gamma}{6 Nu}$$

APPENDIX B
SOLID PROPERTIES

APPENDIX B
SOLID PROPERTIES

B-1: Solid Composition

Due to trade secrets the exact composition of the solid is unknown. An approximate composition believed to be :

	<u>Weight %</u>
Alumina	90
Silica	7
Magnesia	1
Calcia	1
Iron	1

From Reference (12), the heat capacity of each component is found. The heat capacity of the solid was calculated using the weight percent as an averaging factor.

$$C_s = .9 C_{Al_2O_3} + .7 C_{SiO_2} + .1 C_{MgO} + .1 C_{CaO} + .1 C_{Fe}$$

$$C_s = 2.432133 \times 10^{-2} + 7.3507159 \times 10^{-4} (T) - 6.950511 \times 10^{-7} (T^2) + 2.2368314 \times 10^{-10} (T^3), \text{ kCal/g K}$$

The calculated value of C_s at 100°C was found to differ by 3% from the value reported in Coors Ceramics bulletin No. 953.

B-2: Solid Thermal Conductivity

Thermal conductivity data for AD-90 was taken from Coors Ceramics bulletin No. 953 and fitted into a third order polynomial.

$$\lambda_s = 17.691246 - .05338163(T) + .899576T^3 \times 10^{-4} (T) \\ - .17018777 \times 10^{-7} (T^3)$$

where T is in $^{\circ}\text{C}$ and λ_s in w/m K

B-3: Solid Density

The density of the packing was measured and found to be 3510 kg/m^3 at room temperature.

Temperature effects were calculated and found to be negligible (less than 1.5%) (13) Figure 12 showed the thermal expansion curve as a function of temperature.

B-4: Solid Particle Diameter

The particle diameter was found to be 1.837 mm at room temperature. Temperature effects were found to be negligible less than 0.5% (13).

B-5: Bed Void Fraction

The bed void fraction was found to be .349 at room temperature.

B-6: Procedure for Determining Solid Density, Particle Diameter and Void Fraction.

In a 500 ml flask, place enough spheres to fill the flask to the 500 ml mark. Add enough water to the spheres to fill the flask to the 500 mm mark. Record the volume of water added.

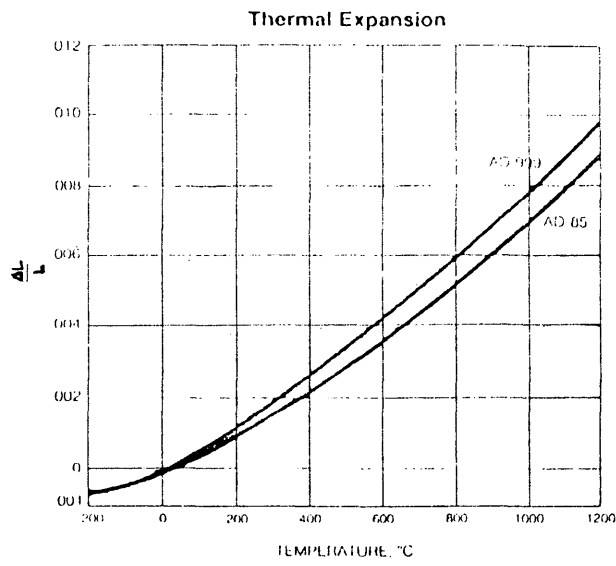


Figure 12. SOLID THERMAL EXPANSION CURVE

The volume of voids is equal to 500 ml minus the volume of water. The void fraction is equal to the ratio of the volume of the voids to the total volume.

Weigh the spheres.

The density of the solid is equal to the ratio of the mass of the spheres to their volume. The volume of the spheres is equal to the total volume minus the volume of water.

Weigh a number of spheres (500). Calculate the average weight of one sphere. Calculate the volume of one sphere. The volume of one sphere is equal to the mass of one sphere multiplied by the density. Calculate the average diameter of one sphere.

B-7: Solid Emissivity

The solid emissivity (ρ) used in the calculation of the solid-solid and void-void radiation heat transfer coefficients was 0.35. The value was taken from reference (17) for a grain size of 4 μ .

APPENDIX C
FLUID PROPERTIES

All nitrogen properties are taken from Reference (7). In the case when they are not available at the temperature required, the values listed are extrapolated linearly. All properties except density are at 1 atm.

APPENDIX D
INSULATION PROPERTIES

Figure 13 shows the thermal conductivity of the insulation as a function of temperature and density.

Corablanke, Corafelt and Corachrome Felt

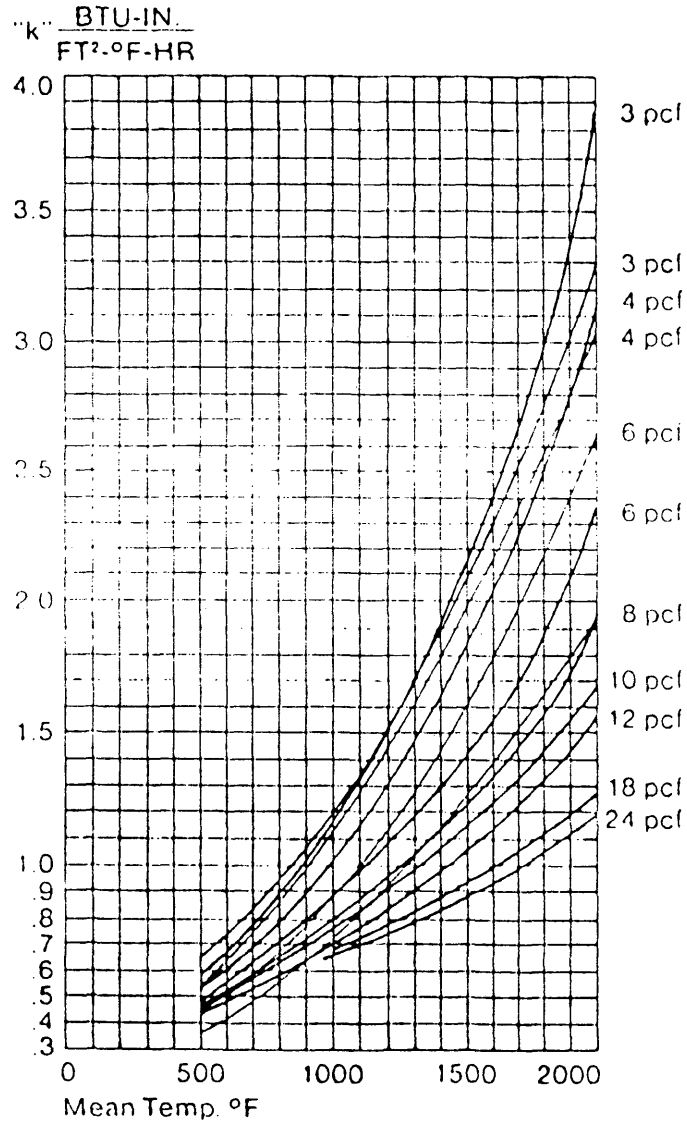


Figure 13. THERMAL CONDUCTIVITY OF THE INSULATION

APPENDIX E
COMPUTER PROGRAM

APPENDIX E

The computer program developed for the solution of the modified one phase mode utilized the implicit method of solution of partial differential equations.

In the program the finite difference approximations for the different partials were the following:

$$\frac{\partial T}{\partial t} = \frac{T_i^{n+1} - T_i^n}{\Delta t}$$

$$\frac{\partial T}{\partial x} = \frac{T_{i+1}^{n+1} - T_i^{n+1}}{\Delta x}$$

$$\frac{\partial^2 T}{\partial x^2} = \frac{T_{i+1}^{n+1} - 2T_i^{n+1} + T_{i-1}^{n+1}}{(\Delta x)^2}$$

By substituting the partials by their equivalent finite difference approximations a set of linear simultaneous equations was obtained for each node i in which the temperature at the new time $n+1$ was calculated. The Thomas algorithm (11) was used to solve the set of equations at each new time.

The boundary conditions used were

1. At the inlet: The fitted polynomial of the response of the inlet thermocouple was used to calculate the temperature at the first node at each new time.
2. At the outlet: The boundary condition used was:

$$\frac{\partial T}{\partial x} = 0 = \frac{T_{i+1}^{n+1} - T_i^{n+1}}{\Delta x}$$

which implied that:

$$T_{i+1}^{n+1} = T_i^{n+1}$$

That was done to find the temperature at a fictitious node outside the bed.

```

C
C   SOLUTION OF DIFFERENTIAL EQUATION
C   FOR PACKED BED USING ONE PHASE
C   MODEL AS SUGGESTED BY VORTMEYER (1).
C   THIS PROGRAM TAKES INTO ACCOUNT
C   HEAT LOSS FROM THE BED
C
C   ***** IMPLICIT METHOD *****
C
C   DIMENSION TNEW(100), TOLD(100), TFIT(100)
C   DIMENSION AA(100), BB(100), CC(100), S(0:10), P(0:10)
C   DOUBLE PRECISION TIMES,DTS
C
C   WRITE(4,102)
102  FORMAT(' ENTER PECLET NUMBER AND GAMMA ')
    READ (4,101) PE,GAMMA
106  FORMAT(1G)
C
    WRITE(4,103)
103  FORMAT(' ENTER DIMENTIONLESS TIME AND
1   NUMBER OF NODES ')
    READ(4,101) DTS,M
101  FORMAT(2G)
    WRITE (4,104)
104  FORMAT(' ENTER THE HIGHEST ORDER OF POLYNOMIAL FIT '/
1   ' FOR INLET AND OUTLET TEMPERATURES ')
    READ(4,106) N
    DO 2 I=1,N+1
      K=I-1
    WRITE(4,109) K,K
109  FORMAT(' ',' ENTER COEFFICIENT A(',I3,')',5X,'B(',I3,')')
    READ(4,101) S(K), P(K)
2    CONTINUE
C
C
C   WRITE(4,105)
    READ(4,106) H
105  FORMAT(' ',' ENTER H ')
    WRITE(4,110)
110  FORMAT(' ENTER MAXIMUM TIME (DIMENTIONLESS X10-4)')
    READ(4,106) TIMAX
    WRITE(4,112)
112  FORMAT(' ENTER THE TIME BEFORE WHICH OUTLET IS '/
1   ' ZERO (DIMENTIONLESS X10-4)')
    READ(4,106) TIMIN
C
C   CALCULATE DXS, THE SPACE INTERVAL
C   THE LENGTH OF THE BED IS .103 METER.
C   THE PARTICLE DIAMETER IS 1.837E-03
C   M IS THE NUMBER OF NODES.

```

```

C
1000 DXS=.103/(1.837E-03*M)
C
C   SET ITERATION COUNTER, TIME,
C   AND SUM OF DIFFERENCE SQUARE
C   (EPS) TO ZERO.
C   THE VOID FRACTION (IN DELTA)
C   IS .349
C
C   TIMES=0.0
C   COUNT=0.0
C   ITER=0
C   EPS=0.0
C   DELTA=1.0/(PE*(1.0-.349))
C
C   CALCULATE CONCTANTS FOR FINITE
C   DIFFERENCE EQUATION.
C   C1=-DELTA*DTS/(DXS**2)
C   C2=-2.*C1+GAMMA*DTS/DXS+H*DTS+1.
C   C3=C1-GAMMA*DTS/DXS
C   C6=C2+C1
C
C   INPUT ELEMENTS OF TRIDIAGONAL MATRIX
C
C   AA(2)=0.
C   AA(M)=C3
C   BB(2)=C2
C   BB(M)=C6
C   CC(2)=C1
C   CC(M)=0.
C
C   DO 20 I=3,M-1
C   AA(I)=C3
C   BB(I)=C2
C   CC(I)=C1
20  CONTINUE
C
C   INPUT INITIAL TEMPERATURE DISTRIBUTION
C
C   DO 10 I=1,M
C   TOLD(I)=0.
10  CONTINUE
C
C   INCREMENT TIME AND CHECK IF IT
C   IS GREATER THAN THE REQUIRED
C   TIME FOR THE RUN.
C
1   TIMES=TIMES+DTS
   TIME=TIMES*1.E-04
   IF(TIME.GT.TIMAX) GO TO 500
C

```

```

C      CALCULATE NEW TEMPERATURE FOR THE
C      FIRST NODE AND THE CONSTANT FOR
C      THE SECOND NODE.
C
      TNEW(1)=S(0)+TIME*(S(1)+TIME*(S(2)+TIME*(S(3)+TIME*(S(4)
1    +TIME*(S(5)+TIME*(S(6))))))
      TOLD(2)=TOLD(2)-C3*TNEW(1)
C
C      CALL SUBROUTINE TRIDAG TO CALCULATE
C      NEW TEMPERATURE PROFILE.
C
      CALL TRIDAG(2,M,AA,BB,CC,TOLD,TNEW)
C
C
      COUNT=COUNT+1.
      IF (COUNT.EQ.50.0) GO TO 11
      GO TO 50
11     COUNT=0.
C
      WRITE(1,101) TIME,TNEW(1)
      *WRITE(7,101) TIME,TNEW(M)
      TFIT(M)=P(0)+TIME*(P(1)+TIME*(P(2)+TIME*(P(3)+
1    TIME*(P(4)+TIME*(P(5)+TIME*(P(6))))))
      IF(TIME.LT.TIMIN) TFIT(M)=0.0
      WRITE(2,101) TIME, TFIT(M)
      DIFR=(TNEW(M)-TFIT(M))**2
C
C      SUM THE SQUARES OF THE DIFFERENCES
C      BETWEEN THE FITTED AND CALCULATED
C      TEMPERATURE FOR NODE M.
C
      EPS=EPS+DIFR
      GO TO 50
C
500   WRITE(4,107) PE, EPS
107   FORMAT(' END OF CALACULATIONS FOR PE=',F10.2,5X,'EPS=',E12.7)
      STOP
40    CONTINUE
50    DO 60 I=1,M
      TOLD(I)=TNEW(I)
60    CONTINUE
      GO TO 1
      END
C
C      SUBROUTINE FOR SOLVING A SYSTEM OF LINEAR SIMULTANEOUS
C      EQUATIONS HAVING A TRIDIAGONAL COEFFICIENT MATRIX
C
C      REFERENCE CARNAHAN, LUTHER AND WILKES P446
C

```

```
      SUBROUTINE TR1DAG(IF, L, A, B, C, D, V)
      DIMENSION V(L), A(L), B(L), C(L), D(L),
1      BETA(101), THETA(101)
C
      BETA(IF)=B(IF)
      THETA(IF)=D(IF)/BETA(IF)
      IFP1=IF+1
      DO 1 I=IFP1,L
1      BETA(I)=B(I)-A(I)*C(I-1)/BETA(I-1)
      THETA(I)=(D(I)-A(I)*THETA(I-1))/BETA(I)
C
      V(L)=THETA(L)
      LAST=L-IF
      DO 2 K=1,LAST
2      I=L-K
      V(I)=THETA(I)-C(I)*V(I+1)/BETA(I)
      RETURN
C
      END
```